Nanoscale

RSC Publishing

PAPER

View Article Online
View Journal

Unprecedented inhibition of tubulin polymerization directed by gold nanoparticles inducing cell cycle arrest and apoptosis†

Cite this: DOI: 10.1039/c3nr33891f

Diptiman Choudhury,‡§[a] Paulrajpillai Lourdu Xavier,§[c] Kamalesh Chaudhari,[d] Robin John,[c] Anjan Kumar Dasgupta,[b] Thalappil Pradeep*[c] and Gopal Chakrabarti*[a]

The effect of gold nanoparticles (AuNPs) on the polymerization of tubulin has not been examined till now. We report that interaction of weakly protected AuNPs with microtubules (MTs) could cause inhibition of polymerization and aggregation in the cell free system. We estimate that single citrate capped AuNPs could cause aggregation of $\sim 10^5$ tubulin heterodimers. Investigation of the nature of inhibition of polymerization and aggregation by Raman and Fourier transform-infrared (FTIR) spectroscopies indicated partial conformational changes of tubulin and microtubules, thus revealing that AuNP-induced conformational change is the driving force behind the observed phenomenon. Cell culture experiments were carried out to check whether this can happen inside a cell. Dark field microscopy (DFM) combined with hyperspectral imaging (HSI) along with flow cytometric (FC) and confocal laser scanning microscopic (CLSM) analyses suggested that AuNPs entered the cell, caused aggregation of the MTs of A549 cells, leading to cell cycle arrest at the G_0/G_1 phase and concomitant apoptosis. Further, Western blot analysis indicated the upregulation of mitochondrial apoptosis proteins such as Bax and p53, down regulation of Bcl-2 and cleavage of poly(ADP-ribose) polymerase (PARP) confirming mitochondrial apoptosis. Western blot run after cold-depolymerization revealed an increase in the aggregated insoluble intracellular tubulin while the control and actin did not aggregate, suggesting microtubule damage induced cell cycle arrest and apoptosis. The observed polymerization inhibition and cytotoxic effects were dependent on the size and concentration of the AuNPs used and also on the incubation time. As microtubules are important cellular structures and target for anti-cancer drugs, this first observation of nanoparticles-induced protein's conformational change-based aggregation of the tubulin–MT system is of high importance, and would be useful in the understanding of cancer therapeutics and safety of nanomaterials.

Received 30th November 2012
Accepted 11th March 2013

DOI: 10.1039/c3nr33891f

www.rsc.org/nanoscale

1 Introduction

Inadequate understanding of how nanoparticles (NPs) interact with live cellular structures and concomitant effects of such interactions has been one of the major impediments in realizing the promises of nanotechnology to revolutionize biology and medicine.[1–18] Because of the high surface area, inherent energy, chemical potential and different surface chemistry of particles as well as protecting ligands, NPs tend to interact with surrounding species to reduce their energy. Often these interactions lead to distinct changes in the interacting system. If proteins happen to be the surrounding species, interaction with NPs leads to altered conformation, aggregation and loss of functionality in a few cases.[1,3–5] Nevertheless, NPs are also affected by certain consequences due to the interaction of proteins on their surface, such as aggregation, etching and dissolution which would influence their stability and functionality.[1] Various studies focusing on nano–bio interactions have shown that NPs induce undesirable protein conformational changes, including increasing the rate of protein fibrillation in the case of amyloid fibrils and loss of protein function.[5–9] Here, one may note that protein misfolding has been the leading reason in certain neuronal diseases such as

[a]Department of Biotechnology and Dr B. C. Guha Centre for Genetic Engineering and Biotechnology, University of Calcutta, 35 Ballygunge Circular Road, Kolkata, West Bengal, India 700019. E-mail: gcbcg@caluniv.ac.in

[b]Department of Biochemistry, University of Calcutta, 35 Ballygunge Circular Road, Kolkata, West Bengal, India 700019

[c]DST Unit of Nanoscience and Thematic Unit of Excellence, Department of Chemistry, Indian Institute of Technology Madras, Chennai, Tamil Nadu, India 600036. E-mail: pradeep@iitm.ac.in

[d]Department of Biotechnology, Indian Institute of Technology Madras, Chennai, Tamil Nadu, India 600036

† Electronic supplementary information (ESI) available: TEM images, UV-Vis spectra of AuNPs, IC_{50} plot, cell-viability, FT-IR, HSI spectra and spectral images and confocal images of AuNP-treated MCF-7 cells. See DOI: 10.1039/c3nr33891f

‡ Current address: Department of Medicine, Division of Uro-Oncology, Cedars Sinai Medical Centre, 8700-Bevarly Blvd, Los Angeles, California 90048, USA.

§ These authors contributed equally to this work.

Alzheimer's, Parkinson's and bovine spongiform encephalopathy (BSE), a prionic disease.[7,8] Formation of sub-nanometer sized particles in protein templates also leads to conformational change.[10] Halas *et al.* have shown that weakly protected AuNPs caused protein based aggregation of lysozyme at physiological pH.[9] Like NP–protein interaction, knowing how NPs interact with live cells and cellular organelles has been of paramount importance and is indeed a natural extension of the problem mentioned earlier.[12–19] Various NP–cell interactions have exhibited undesirable outcomes, sometimes resulting in disruption of organelles and cell death.[12,15] Au based nanostructures have been one of the promising nanosystems as far as the bio-medical field is concerned.[18–26] Recently, various studies of AuNPs interaction with cells have shown that AuNPs, once believed to be biocompatible, showed unexpected toxicity to human cells under certain conditions.[27–31] Hussain and coworkers studied the surface charge dependent toxicity of AuNPs.[28] We have earlier reported that citrate capped gold nanoparticles without any functionalization can be selectively toxic to lung carcinoma (A549) cells while baby hamster kidney (BHK21) and human hepatocellular liver carcinoma (HepG2) cells remained unaffected; however the molecular mechanism of the toxicity remains unknown.[27] While most studies have addressed the NP–extracellular protein interaction, very few studies have focused on the interaction of AuNPs with intracellular proteins, especially with the cytoskeletal proteins.[4,14,43–46]

Among the numerous intracellular proteins, tubulin is an important cytoskeletal, heterodimeric globular-protein containing α and β subunits, with nearly 20 free thiols. It is involved in microtubule (MT) formation, shows dynamic instability, is responsible for intracellular transport of cargos and several signalling mechanisms, and has been the most desired target to treat cancer.[32] Various drugs have been used to target the tubulin–MT equilibrium.[33,34] Tubulin–MT equilibrium targeting drugs alter the dynamics in two different ways, either by stabilizing the polymer structure of MT as in the case of taxol[35] or by inhibiting the tubulin polymerization into MT as in the case of vinblastine and vitamin K3.[36,37] Several of the tubulin–MT targeting agents show cell cycle arrest at the G_2/M phase of the cell cycle.[38] Among them taxol and colchicine are well-known anti-MT agents. Some of the compounds also show cell cycle arrest at the G_0/G_1 phase. These compounds mainly disrupt the interphase MT network of the cells. For instance, a low concentration of colcemid does not cause disruption of spindle MT or show cell cycle arrest at the G_2/M phase, instead it disrupts inter-phase MT and shows cell cycle arrest at the G_0/G_1 phase.[39–42] Very few studies have been done specifically on tubulin–NP interaction. The studies we came across are: alteration of the position of tryptophan residues in MT by TiO_2 NPs,[43] fabrication of AuNPs in MT filaments polymerized by taxol[44] and remodelling of MT (through acetylation) by reactive oxygen species produced by Fe_2O_3 NPs[45] and recently, a docking study of fullerene interaction with MT.[46] The so-far unaddressed interaction between AuNPs and tubulin and the elusive toxicity mechanism of citrate capped non-functionalized AuNPs in A549 cells[27] have prompted us to carry out this study. We hypothesized that interaction with tubulin could likely result in the toxicity observed, as it has 20 free thiols (since thiols have strong affinity for gold). Hence, we carried out a two phase study investigating the influence of AuNPs on (i) the microtubule assembly *in vitro*, (ii) the microtubule system and the cell cycle in A549 cells.

As experimental outcomes, in this study, to the best of our knowledge till date, for the first time, we report AuNPs-induced conformational change-based inhibition of polymerization and aggregation of tubulin–MT in the cell free system. This is distinctly a new observation as far as the interaction of AuNPs with the tubulin–MT system is concerned. We have also observed AuNPs-induced MT damage-mediated cell cycle arrest at the G_0/G_1 phase and cellular apoptosis in A549 cells *in vitro*. In this study we have carried out experiments using TEM, dark-field microscopy and FTIR, Raman, UV-Visible, fluorescence spectroscopic and molecular biological techniques to know how AuNPs change the tubulin–MT protein equilibrium in a cell free system and in a cancer cell. This study, we believe, would provide a new insight into the intracellular protein–AuNPs interaction and associated toxicity, and also be useful in understanding the safety of nanomaterials.

2 Experimental section

2.1 Materials

Hydrogen tetrachloroaurate ($HAuCl_4 \cdot 3H_2O$), sodium citrate, DAPI, DTNB, mice monoclonal anti-human α tubulin antibody without conjugation, goat monoclonal anti-mouse IgG antibody with rhodamine conjugation, GTP, PIPES, EGTA, RNase A, PI (propidium iodide) and KBr were purchased from Sigma, USA. Nutrient Ham's F12 (supplemented with 1 mM L-glutamine), bovine fetal serum, penicillin–streptomycin mixture and 100 mM fungizone were purchased from HyClone, USA. Trypsin–Versene was purchased from Cambrex Bioscience, USA. Bradford Protein estimation kits were purchased from GeNei, India. Annexin V-FITC apoptosis detection kit was obtained from BD Biosciences, San Diego, CA, USA. The Folin–Ciocalteu reagent and other chemicals of analytical grade were purchased from Sisco Research Laboratories, India.

2.2 Instrumentation

All scattering and absorbance measurements were performed using a UV-Visible spectrophotometer (JASCO V-630) equipped with a variable temperature water bath. The plasmonic shift of NPs was studied using a Perkin Elmer Lambda 25 spectrometer equipped with a variable temperature water bath. All fluorescence measurements were performed using a Photon Technology International Fluorescence spectrophotometer (USA) equipped with a variable temperature Peltier system, and data were analyzed using FeliX32 software. Electron microscopy analysis was done using a JEOL 3010 HRTEM. CD spectroscopic measurements were done using a JASCO CD spectrophotometer J-815. The confocal Raman microscope used was a CRM Alpha 300S (manufactured by WITec, GmbH, Germany) with a 532 nm laser. The excitation laser was focused using a 100× objective,

and the signal was collected in a back scattering geometry and sent to the spectrometer through a multimode fiber. Cell cycle experiments were performed using a Becton Dickinson FACS Calibur, and the data were analyzed using CellQuest program from Becton Dickinson. Bright field images were taken of cells by an Olympus inverted microscope model CKX41. Confocal images were taken with a Zeiss LSM 510 Meta Confocal Laser Scanning Microscope and images were processed with LSM software. Dark field microscopy experiments were done using a Cytoviva microscope, attached to a hyperspectral imaging system. The system captures the VNIR (400–1000 nm) spectrum within each pixel of the scanned field of view and spectral image analysis was done using ENVI software.

2.3 Preparation of AuNPs and purification of mammalian tubulin

AuNPs were prepared by the citrate reduction method. Auric chloride ($HAuCl_4 \cdot XH_2O$) 250 μM was reduced with various concentrations (depending upon size requirements) of tri-sodium citrate.[47] The excess citrate was removed by centrifugation and removing the supernatant and resuspending in water. This procedure was repeated thrice. The particle concentration in molarity (M_{NP}) of AuNPs was determined using the following formula (1). Detailed calculations are given in the ESI,† 1A.

$$M_{NP} = \frac{(\text{molarity of } Au^{3+} \text{ in the solution}) \times (\text{volume of one gold atom})}{(\text{volume of one nanoparticle})} \quad (1)$$

Goat brain tubulin was purified by a temperature-dependent polymerization and depolymerization method.[61,62] Finally, the protein was dissolved in PEM (containing 50 mM PIPES, 1 mM EGTA, and 1 mM $MgSO_4$) buffer at pH 6.9. The protein concentration was estimated using the Bradford Reagent[48] using bovine serum albumin as the standard and further confirmed by the DTNB titration method.[49] The protein was stored at −85 °C for further experiments.

2.4 Polymerization inhibition and aggregation studies

Tubulin (12 μM) was incubated at room temperature in the presence of $AuNP_{40}$ and the extinction spectra were monitored. Purified mammalian tubulin (12 μM) was mixed with 15 pM AuNPs ($AuNP_{20}$, $AuNP_{40}$ and $AuNP_{60}$) and polymerized in PEM–glycerol buffer (50 mM PIPES, 1 mM EGTA, 1 mM $MgSO_4$ and 33% glycerol) at 37 °C just after adding 1 mM GTP in the assembly mixture. The rate and extent of the polymerization reaction were monitored by light scattering at 350 nm.[50–52] Tri-sodium citrate in the corresponding buffer was used as the vector for the control sample. To see the effect of various concentrations of $AuNP_{40}$ on tubulin polymerization, purified tubulin (12 μM) was polymerized in the presence of different concentrations (0, 5, 12.5 and 25.0 pM) of $AuNP_{40}$ and the extent of polymerization was monitored in the same way as before.[51,52] To study the change of the intrinsic fluorescence of tryptophan residues, 1 μM tubulin was incubated with 15 pM of AuNPs at 25 °C. Fluorescence data were corrected for the inner filter effect according to the equation of Lakowicz,[53] $F = F_{obs}\,\text{antilog}(A_{Ex} + A_{Em})/2$ where A_{Ex} stands for the absorbance at the excitation wavelength (295 nm) and A_{Em} stands for the absorbance at the emission wavelength (335 nm). For HRTEM analysis 12 μM tubulin was polymerized in PEM–glycerol buffer in the absence and presence of 25.0 pM $AuNP_{40}$. Samples were then fixed with 0.25% (v/v) glutaraldehyde. Each sample (10 μL) was then loaded on 300 mesh carbon coated copper grids. The samples were allowed to stand for 5 min, and after washing, grids were negatively stained with 2% uranyl acetate. Copper grids were dried under vacuum, and the samples were viewed using TEM.[40] Samples used for TEM were also used for hyper-spectral imaging (dark field microscopy). Samples were spotted on glass coverslips and then air dried for 30 minutes. Pictures were taken using a Cytoviva microscope at 100× magnification.

2.5 Study on the effect of AuNPs on polymerized tubulins (MT)

Tubulin heterodimers were allowed to polymerize in the presence of excess GTP (2 mM) at 37 °C. The system was allowed to polymerize till saturation (25 min) and was monitored by scattering at 350 nm. Then different concentrations of 15 μL of $AuNP_{40}$ (5, 12.5 and 25 pM, respectively) and the buffer (AuNP free buffer after centrifugation at 10 000*g* for 20 minutes) was added to the solution and mixed slowly and scattering at 350 nm was monitored for another 25 minutes. Since AuNPs have a strong extinction at 350 nm, nano-particles were also incubated in protein free buffer (PEM–glycerol–GTP) and used for background correction.

2.6 Studies on conformational change

For CD spectroscopic analysis, tubulin (1 μM) was incubated with different concentrations 0, 10, 25 and 50 pM of $AuNP_{40}$ separately in 20 mM sodium phosphate buffer (pH 6.90) for 60 min at 37 °C. Then CD spectra were taken in the range of 200–260 nm wavelength regions. Phosphate buffer was used for CD as PIPES had high absorbance at 220 nm. Thiol estimation was done using the DTNB titration method. Tubulin (1 μM) was incubated with 25.0 pM of $AuNP_{40}$ for 60 min at 37 °C, and then the sample was titrated with 400 μM DTNB (excess) for 15 min separately, and compared with the control. In the first set 12 μM tubulin was polymerized for 30 min at 37 °C in the presence and absence of 25.0 μM $AuNP_{40}$ and in the second set, 12 μM tubulin was incubated for 3 h at 37 °C (in an unpolymerizing condition) in 25.0 pM $AuNP_{40}$ and FTIR spectra were measured for all sets using a Perkin Elmer Spectrum One instrument. KBr crystals were used to prepare the matrix for the samples. The second derivative of the FTIR spectrum was taken using "Spectrum One" software provided by Perkin Elmer. For each set, at least 5 independent experiments were done. 100 μL of each sample used for FTIR analysis was taken and dried (under vacuum) on an inert glass surface for Raman studies. Raman spectra of all samples were taken using 532 nm laser excitation. For each set, at least 5 independent experiments were done. Western blot experiment was carried out as reported elsewhere. 200 μg of the whole cell extract was used as samples for cell free and

intracellular tubulin systems, respectively. Samples were given cold shock before running the gel. Control and treated A549 cellular protein were collected after cold induced depolymerization for 6 h at 4 °C. Western blot was done after running 6% non-reducing SDS PAGE, using mouse monoclonal anti-α-tubulin antibody as the primary and HRP conjugated goat monoclonal anti-mouse IgG as the secondary antibody. Protein bands were detected in X-ray films using the chemiluminescence technique. Anti-actin and anti-GADPH antibodies were used for the detection in the experiment.

2.7 *In vitro* cell line experiments

Human lung carcinoma A549 and human breast cancer MCF-7 cells were maintained in Ham's F12 supplemented with 1 mM L-glutamine, 10% fetal bovine serum, 0.2% $NaHCO_3$, 1 mM penicillin, 1 mM streptomycin and 1 mM fungizone pH 7.4. Cells were cultured at 37 °C in a humidified atmosphere containing 5% CO_2. Fresh media as well as fresh AuNPs were added every 24 h of the treatment. For each dose, approximately 1×10^6 cells were taken in a 35 mm tissue culture plate and each experiment was repeated at least 5 times.[40,51,52] To analyse the cytotoxic effects of AuNPs, 25 pM of $AuNP_{20}$, $AuNP_{40}$ and $AuNP_{60}$ were incubated for 72 h and the cell viability assay was performed by a trypan blue viable cell count method.[40] For each set, at least 5000 cell counts were taken. To analyse the effect of $AuNP_{40}$ on cell cycle progression, cultured A549 cells were treated with different concentrations of $AuNP_{40}$ (12.5 and 25.0 pM) along with the control for 72 h. After the treatment, cells were fixed with methanol and treated with RNase A and then stained with propidium iodide and cell cycle analysis was carried out in a flow cytometer. To study the apoptotic effect, $AuNP_{40}$ (12.5 and 25.0 pM) treated cells were processed with fluorescence isothiocyanate (FITC)-conjugated Annexin V for 15 minutes at room temperature in a calcium enriched buffer. Propidium iodide (PI) was used as the counter stain for flow cytometric analysis. To study the effect of $AuNP_{40}$ on cellular morphology, A549 cells were grown on coverslips at a concentration around 1×10^5 cm^{-2} and treated with $AuNP_{40}$ as previously mentioned and bright field images were taken. MTs of A549 cells were stained using mouse monoclonal anti-α-tubulin antibody (Sigma) at 1 : 100 dilution and rhodamine conjugated goat monoclonal anti-mouse IgG secondary antibody (Santa Cruz Biotechnology) at 1 : 150 dilution. After staining, confocal images were taken. The cells were treated for a period of 12 h, and 24 h with 25 pM of $AuNP_{40}$ on glass slides in an animal cell culture plate. Images were taken after repeated 1× PBS wash at 37 °C using a halogen lamp (400–1000 nm) as the light source at 100× magnification.

3 Results and discussion

3.1 Structural changes due to tubulin AuNP interactions in a cell free system

Citrate capped spherical AuNPs with sizes of 20 nm ($AuNP_{20}$), 40 nm ($AuNP_{40}$) and 60 nm ($AuNP_{60}$) were prepared by a standard method.[47] AuNP sizes were calculated from the observed extinction coefficients in UV-Vis spectroscopic studies and were further confirmed by electron microscopic studies (Fig. S1†). The polymerization reaction mixture containing 12 μM of tubulin was incubated with 15 pM AuNPs and the surface plasmon resonance (SPR) was monitored by UV-Vis spectroscopy (Fig. 1).

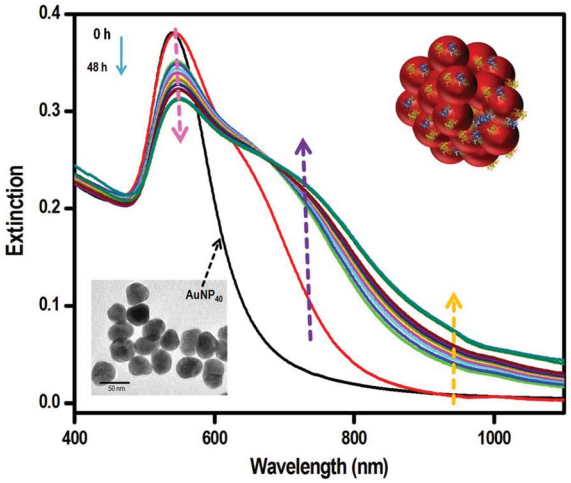

Fig. 1 Structural changes of $AuNP_{40}$ due to interaction with tubulin: shift of SPR of $AuNP_{40}$ (black solid line) from 532 nm to 540 nm (red solid line) due to the initial association of tubulin and change of the dielectric constant of the environment. As a function of incubation time with tubulin, while the SPR intensity at 540 nm decreases, a new plasmon peak, possibly due to closely spaced NPs appears in the near infrared at 750 nm (purple dotted arrow). The increase in the background signal near 1000 nm (yellow dotted arrow) indicates aggregation. Inset (down, left): TEM image showing parent $AuNP_{40}$ (scale bar is 50 nm). Inset (up, right): schematic representation of the closely spaced nanoparticles in association with the protein molecules.

We observed a slight 8 nm red shift, immediately upon the addition of $AuNP_{40}$ to the tubulin mixture which is likely to be due to the change in the dielectric constant of the nanoparticle's environment, induced by the surrounding proteins. As a function of time, while we observed a decrease in the SPR of $AuNP_{40}$ at 540 nm, there was an increase in the absorbance in the NIR region with a single isosbestic point at 683 nm and a new plasmonic peak developed around 750 nm. Increase in the background signal near 1000 nm was also observed which can be attributed to close spacing of AuNPs or aggregation[9,54] (Fig. 1). The presence of a single isosbestic point suggests the involvement of a single intermediate state between the two forms of particles (single particles and protein induced aggregated ones).

To know the fate of the protein's functionality due to the interaction, we monitored the scattering[50] at 350 nm for 30 minutes which corresponds to polymerization of tubulin into MT. Results suggested that AuNPs inhibited the polymerization process significantly. Among the three different sized NPs used for the experiment, $AuNP_{40}$ showed maximum inhibition of polymerization to the extent of 46.13 ± 3.1% while $AuNP_{20}$ and $AuNP_{60}$ showed 12.87 ± 3.2% and 23.91 ± 4.1%, respectively (Fig. 2A) (Table 1). Since $AuNP_{40}$ showed high polymerization inhibition, we chose this system for further microscopic and

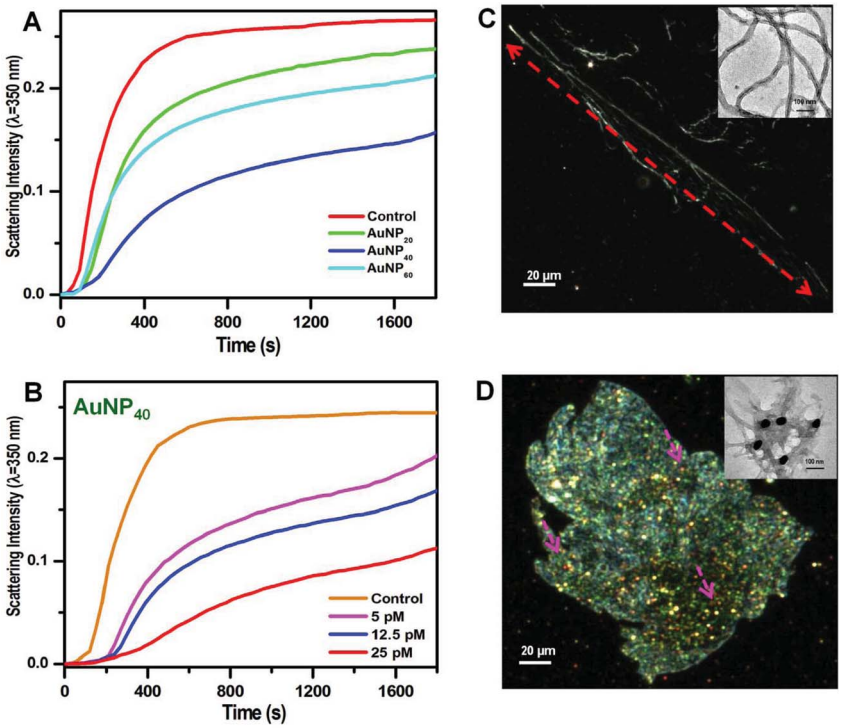

Fig. 2 Effect of AuNPs on the polymerization of purified mammalian tubulin: (A) plots showing the inhibition of polymerization by three differently sized AuNPs. $AuNP_{40}$ (blue solid line) shows maximum initial delay and inhibition of polymerization. (B) $AuNP_{40}$ shows concentration-dependent inhibition of polymerization. (C) Dark field microscopic image (scale bar 20 μm) of polymerized tubulin (MT) in the absence of $AuNP_{40}$ (the red-dotted double sided arrow indicates the formation of long MT). The inset is a transmission electron microscopic (TEM) image (scale bar 100 nm) showing polymerized MT stained with uranyl acetate in the absence of $AuNP_{40}$. (D) In the presence of 25 pM $AuNP_{40}$, MT was not formed, instead extended amorphous aggregates were formed. The dark field microscopic image (scale bar 20 μm) shows one such large aggregate; bright yellow, red and blue spots are $AuNP_{40}$ particles (magenta dotted arrows point at AuNPs) and the inset TEM image (scale bar 100 nm) shows the nanoparticle-induced protein aggregation. Note that very few NPs cause aggregation of a huge number of protein molecules.

spectroscopic studies to probe the reason behind the inhibition of polymerization.

We further studied the concentration dependent inhibition of polymerization by $AuNP_{40}$ at 5.0, 12.5 and 25.0 pM concentrations which exhibited respectively, $28.6 \pm 2.7\%$, $40.32 \pm 1.7\%$ and $60.47 \pm 3.5\%$ inhibition (Fig. 2B) (Table 2). From these observations, we calculated the concentration required for 50% inhibition of polymerization.

The calculated IC_{50} was 18.6 ± 0.9 pM (Fig. S2†) and the molar ratio between $AuNP_{40}$ and tubulin was $1 : 3.16 \times 10^5$ (see the ESI† for the calculation). This implies that a single AuNP is enough to create an avalanche of aggregation when coming in contact with tubulin inside a cell. In order to observe the aggregates, we carried out hyper-spectral imaging using dark field microscopy and TEM studies of tubulin–reaction mixtures with and without $AuNP_{40}$, incubated for the formation of MT. Reaction mixtures without $AuNP_{40}$ formed long fiber-like structures of MT (Fig. 2C) (the inset shows a TEM image), while the reaction mixture with 25 pM $AuNP_{40}$ formed random tubulin aggregates. The association of the nanoparticles with protein aggregates is clear from the figures. In the hyper-spectral image, the red and yellow spots show that they are nanoparticles (Fig. 2D). The inset of the figure shows a TEM image of a portion of such an aggregate. Since we observed that a single nanoparticle could cause 10^5 tubulin molecules to aggregate (Fig. S2†) and all protein molecules could not have interacted with the available AuNPs, there must be a conformational-change-based protein aggregation mechanism, as observed in some neuronal diseases and previous studies.[7,8] To test whether the inhibition of polymerization and aggregate formation (Fig. 2) are due to conformational changes caused by AuNPs, we probed the conformational changes of the protein by a set of standard analytical techniques. Direct microscopic and UV-Vis spectroscopic studies revealed that $AuNP_{40}$ interacted with purified mammalian tubulin and caused aggregation. But surprisingly, circular dichroism (CD) studies showed very little changes in the conformation of MT (Fig. S3†). Hence, to probe the change, Raman spectroscopic investigation was carried out (Fig. 3). Raman spectroscopy can provide insights into the structural modifications in protein upon its interaction with AuNPs.[9] The amide bonds which link amino acids are amide-I, amide-II and

Table 1 Percentage of inhibition of polymerization of tubulin by three differently sized AuNPs

AuNPs (15 pM)	Absorption maximum (nm)	Size of AuNPs (nm)	Inhibition of polymerization (%)
$AuNP_{20}$	525	20	12.87 ± 3.2
$AuNP_{40}$	532	40	46.13 ± 3.1
$AuNP_{60}$	537	60	23.91 ± 4.1

Table 2 Concentration dependent inhibition of polymerization of tubulin by $AuNP_{40}$

Concentration of $AuNP_{40}$ (pM)	Inhibition of polymerization (%)
5.0	28.6 ± 2.7
12.5	40.3 ± 1.7
25.0	60.5 ± 3.5

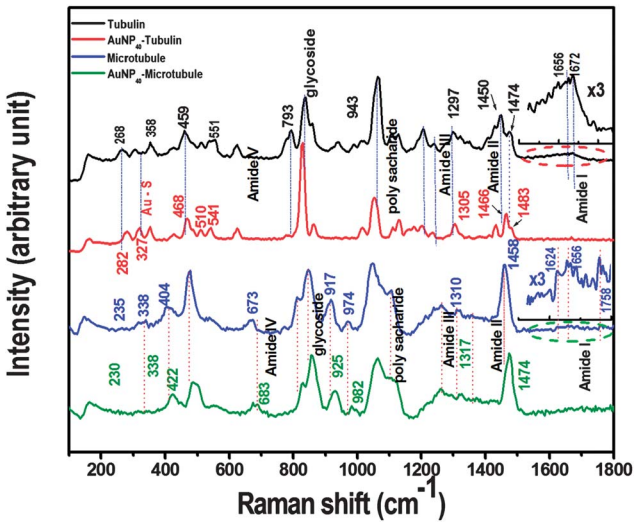

Fig. 3 Raman spectral features for MT and tubulin upon $AuNP_{40}$ treatment: various curves are labelled with the corresponding colors. Important regions (amide-I, amide-II, amide-III, amide-IV, amide-V and glycoside linkage) have been marked by the name of the prominent bond in the region and are discussed in the text and in Table 3. Specific regions are multiplied by 3 to show the features clearly.

amide-III, which give specific vibrational bands in the range of 1600–1690, 1480–1575, 1229–1301 cm^{-1}, respectively.

Other amide vibrational bands come in the range of 625–767 cm^{-1} (OCN bending), 640–800 cm^{-1} (out of plane NH bending), 537–606 cm^{-1} (out of plane C═O bending), and 200–300 cm^{-1} (skeletal torsions) which are assigned as amide-IV, amide-V, amide-VI and amide-VII, respectively.

The amide-I vibrational structure is the most sensitive among all and any alteration of it is a signature for protein secondary structure modification. $AuNP_{40}$ induced some changes in the secondary structures of both the forms (MT and tubulin heterodimer) of the protein. In both the cases, $AuNP_{40}$ altered the protein β sheet regions. In addition to that, alteration at the α-helix region of MT was also observed. Though all the Raman features are not fully understood, alterations in structural features show partial conformational changes. In both sets of our experiment, we observed changes in the protein features (Fig. 3). Each measurement was repeated up to 5 times and in the presence of AuNPs, enhancement in the Raman spectral intensity was observed due to SERS. The Raman feature at 1655 cm^{-1} is due to amide-I (C═O stretching in combination with the contributions from C–N stretching) of the protein's random coiled structure. In the case of tubulin, the shoulder at 1656 cm^{-1} got shifted to a very weak feature at 1668 cm^{-1}, while the other feature at 1672 cm^{-1} disappeared completely upon treatment with AuNPs indicating a possible modification of the secondary structure. In the case of MT, the weak feature at 1656 cm^{-1} disappeared upon interaction with AuNPs. The feature at 1624 cm^{-1} due to the β sheet of MT got shifted to 1628 cm^{-1} upon interaction with AuNPs. The amide II (N–H deformation and contribution from C–N stretching) feature for tubulin β sheets at 1474 cm^{-1} got shifted to 1483 cm^{-1} and the similar feature for MT at 1458 cm^{-1} got shifted to 1474 cm^{-1} during the interaction. The amide II feature for the tubulin α helix at 1450 cm^{-1} was shifted to 1468 cm^{-1}. There was no corresponding feature in the case of MT.[55] Au–S stretching at ~327 cm^{-1} was observed in the $AuNP_{40}$–tubulin sample[56] but was not observed in the AuNP–MT sample; this may suggest that the interaction leading to aggregation requires a specific site or chemical moiety of the tubulin monomer. Since tubulin does not have any disulphide bond, no stretching at 504 or 524 cm^{-1} was observed.[9] Structural modifications upon interaction with AuNPs were observed in various regions like amide III, IV and V and C–O–C bending region (symmetric and asymmetric) as evident from Table 3.

We have also compared FTIR and second derivative FTIR spectra of tubulin and MT before and after interaction with AuNPs. The second derivative of FTIR is sensitive and typically used to analyse the conformational changes in the amide I region of the protein where the changes are difficult to be observed in the primary spectra.[10] Direct comparison of FTIR spectra has not revealed anything significant (Fig. S4†). The amide I (1600–1690 cm^{-1}) band observed is due to characteristic stretching and bending vibrations of the amide bonds, most sensitive to protein secondary structures. Hence we have studied and compared the second derivative of the FTIR spectra in this window (Fig. 4). The band appearing at 1654 cm^{-1} is assigned to the α helix and the bands appearing at 1648 and 1640 cm^{-1} are attributed to disordered α-helices (random coil). The prominent band for β-sheets is observed at 1685 cm^{-1}; it also shows signatures at 1634 and 1627 cm^{-1}. The bands between 1664 and 1682 cm^{-1} are assigned to β-turns.[10] The comparison between spectra of tubulin before and after interaction with AuNPs has shown that there is substantial decrease in the intensity of bands for secondary structures after interaction and is an evidence for the structural changes; such changes could have led to aggregation. However, in the case of MT (polymerized tubulin), no significant changes were observed in the spectra after interaction with $AuNP_{40}$.

In a recent study, Ratnikova *et al.* reported that hydrogen bonding between a tubulin heterodimer and a fullerene derivative can induce conformational change and inhibit polymerization.[46] Hence, not only thiol–Au mediated conformational change, but also interaction of other chemical groups of the protein with AuNPs could contribute to partial conformational change. The exact mechanisms and the chemical moieties involved in these processes would be investigated in detail in a subsequent computational and experimental study.

Each tubulin heterodimer has 12 tryptophan residues which are distributed heterogeneously in α and β-subunits. Direct interaction of a ligand with tubulin may quench the intrinsic

Table 3 Observed Raman shifts (in cm^{-1}) of $AuNP_{40}$-treated MT and tubulin[9,55,56]

MT	$AuNP_{40}$–MT	Possible bond	Tubulin	$AuNP_{40}$–tubulin	Possible bond
235	235	C–C	268	282	C–C
338	338	C–O–C of glycoside		327	Au–S
404	420	—	352	352	—
478	486		427	427	—
528	542	C═O	459	468	
669	673	C═S	551	510	C═O
771	789	O–C–N bending	623	623	C═S
811	824	N–H bending out of plane	793	776	O–C–N bending
847	860	C–O–C	838	829	N–H bending out of plane
917	925	C–O–C	—	864	C–O–C
974	982	Polysaccharide back bones	943	—	C–O–C
1047	1060	Polysaccharide back bones	987	—	Polysaccharide back bones
1107	1102	C–O–C asymmetric	1012	1016	Polysaccharide back bones
1213	1217	Amide III (α helix)	1064	1051	Polysaccharide back bones
1264	1259	Amide III (β sheets)	1107	1111	C–O–C asymmetric
1310	1317	Amide III (random coils)	1128	1128	C═S
1355	1371	C–H bend	1187	1175	—
1458	1474	Amide II (β sheets)	1204	1201	C–C–O stretching
1624	1628	Amide I (β sheets)	1242	1234	Amide III (α helix)
1656	—	Amide I (random coils)	1297	1305	Amide III (β sheets)
—	1700		1322	1326	Amide III (random coils)
1758	—	C═O of alkyl ester	1351	1347	C–H bend
			1450	1468	Amide II (α helix)
			1474	1483	Amide II (β sheets)
			1656	1668	Amide I (random coils)

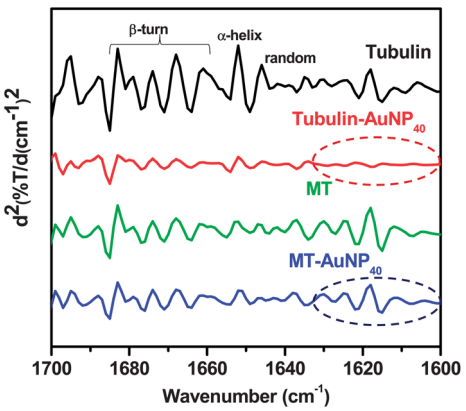

Fig. 4 The second derivative FTIR spectra of the amide I region of tubulin and MT upon interaction with $AuNP_{40}$. Comparisons between specific regions are shown with dotted oval shapes.

tryptophan fluorescence of tubulin. The tryptophan quenching assay (Fig. S5†) also suggested the possibility of the conformational change of the protein upon nanoparticle interaction. Quenching can be due to alteration of the structure or association of AuNPs with the protein (as AuNPs are known to quench fluorescence). Further, as the tubulin heterodimer contains 20 cysteine residues, to monitor the modification of thiol, we did thiol estimation of AuNPs treated tubulin which revealed a loss of 0.6–1 cysteine residues, a loss of 3–5% of the total cysteine content per heterodimer. Even in the case of 25.0 pM $AuNP_{40}$ treatment, we observed only 3–5% loss of the total cysteine content (Fig. S6†). These results indicated that not all thiols are modified and most of them remain free, which further supports the suggestion that conformational change is partial and is reinforced by the Raman spectroscopic observations. To check whether the polymerized tubulins (MT) get depolymerized by the AuNPs (akin to the effect caused by certain MT depolymerising drugs), we monitored the scattering at 350 nm by adding different concentrations of $AuNP_{40}$ to polymerization saturated MT. No significant depolymerization was observed even in the presence of 25 pM of $AuNP_{40}$ (Fig. S7†). These observations further corroborate the results obtained in Raman and FT-IR investigation that polymerized tubulin may undergo lesser conformational changes than free tubulin.

From all the observations made in the cell free system, we have demonstrated that weakly protected AuNPs induce partial conformational changes in tubulin which in turn inhibit polymerization and cause aggregation. One should note that not all proteins undergo such conformational change-based extended aggregation, for example BSA does not get aggregated due to interaction with citrate capped AuNPs;[9,57] thus the observed tubulin aggregation becomes crucial from the point of view of nanotoxicity since it is involved in cellular transport, cell cycle and cell shape stability. Halas *et al.* have also shown that upon protecting the AuNPs with bulky groups such as polyethylene glycol, such extended protein mediated aggregations do not take place.[9] Hence understanding the interaction of bare AuNPs with tubulin becomes crucial. If such an aggregation process happens inside the cell, it is likely to cause cell cycle arrest and apoptosis, and we hypothesized this could be one of the reasons for the selective toxicity observed in the A549 cell line which is a well-known model for microtubule-based studies.

3.2 *In vitro* cell line experiments

To test the above mentioned hypothesis, we incubated the AuNPs of three different sizes (Table 1) for cell viability assay, with the lung cancer cell line (A549), which has a prominent MT network, a widely used cell line in MT targeted drug studies. The cell viability assay results obtained for a 72 h incubation period indicated that $AuNP_{40}$ had the maximum cytotoxicity effect among the three different NPs tested, leaving only 49.86 ± 3.68% of the cells viable while $AuNP_{20}$ and $AuNP_{60}$ left 80.57 ± 4.72% and 59.34 ± 2.75% of cells viable, respectively (Fig. 5A upper panel and Table 4). Cell viability was high for other time intervals, 12, 24 and 48 h, for all three sizes of AuNPs and for different incubation concentrations (Fig. S11†). It has been observed that 40 to 50 nm sized nanoparticles are uptaken more.[58,59] Wei *et al.* observed that 45 nm AuNPs were uptaken more and present in the cytoplasm of lung cancer and HeLa cells using dark field optical sectioning microscopy.[60] This may be the reason for the observed effect: more the uptake, higher the probability of membrane disruption and hence more the probability of toxicity.[61] Since $AuNP_{40}$ caused the maximum cytotoxic effect, we further examined $AuNP_{40}$ treated cells for cell viability, cell cycle arrest, MT damage and apoptosis as a function of its concentration. It indicated that at 12.5 and 25.0 pM of the NPs, 26.0 ± 1.3% and 41.2 ± 2.5% of the cells were in the sub G_0/G_1 phase (hypoploidy) respectively, while only 4.3 ± 0.3% of the control population was in the sub-G_0/G_1 phase (Fig. 5B and C). The calculated IC_{50} value for A549 cells was 29.5 ± 1.7 pM (Fig. S8†). Among a live cell population, the control set had 59.9 ± 1.4% of cells in the G_0/G_1 phase while 12.5 and 25.0 pM $AuNP_{40}$ treated cells had 65.6 ± 1.8% and 71.9 ± 1.1% of the cell population in the G_0/G_1 phase (Fig. 5C and Table 4). These results indicate that AuNPs induce cell cycle arrest at the G_0/G_1 phase (Table 4). To check whether there are onco-cellular apoptosis and cell death pattern, we conducted flow cytometric Annexin V/PI assay. The assay revealed that 72 h incubation of cells with 12.5 and 25.0 pM $AuNP_{40}$ resulted in 22 ± 1% (early = 16.07 ± 0.26% and late = 5.72 ± 0.57%) and 47 ± 1.5% (early = 30.85 ± 0.7 and late = 17.68 ± 0.91%) apoptotic populations, respectively, while the control had only 3 ± 0.5% (early = 2.39 ± 0.23% and late = 0.7 ± 0.14%) apoptotic population (Fig. 5D). Further, investigation of cell

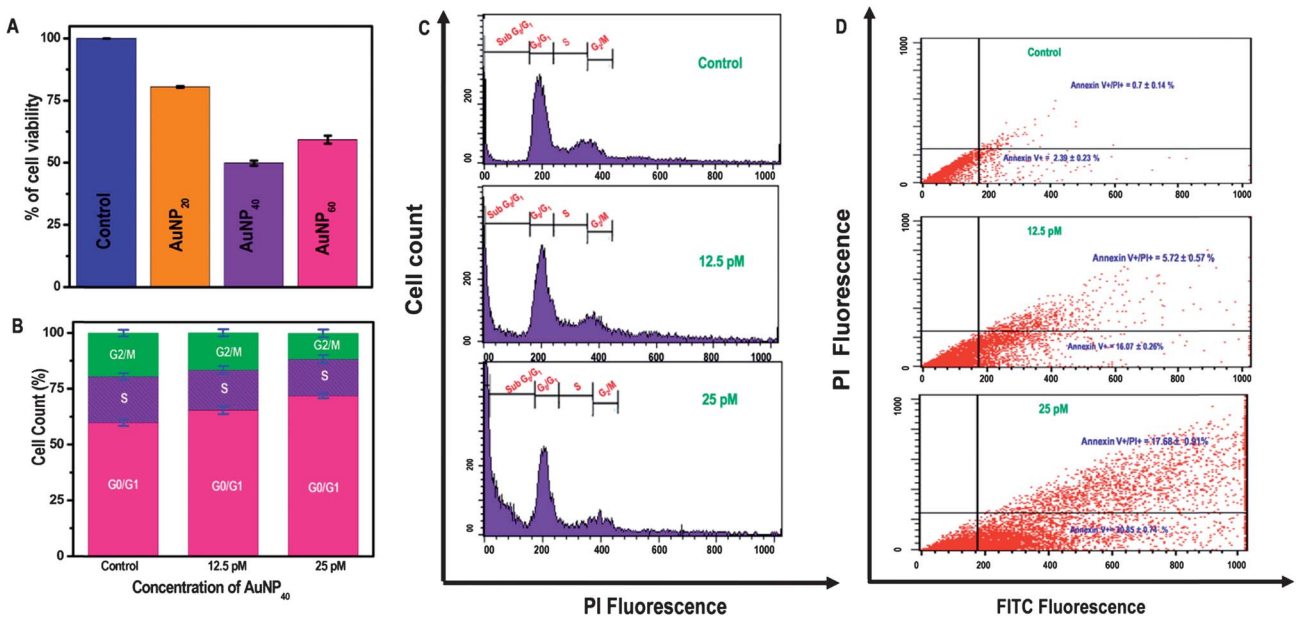

Fig. 5 Effect of AuNPs on cell viability and cell cycle distribution pattern: (A) percentage of cell viability upon incubation with 12.5 pM AuNPs of different sizes for 72 h. (B) Histogram showing cell cycle phase distribution of residual live cells after 72 h of $AuNP_{40}$ treatment (C). FACS data revealing G_0/G_1 cell cycle arrest and induction of A549 cell death after incubation with different concentrations (0, 12.5 and 25.0 pM) of $AuNP_{40}$ for 72 h. (D) Annexin V/PI assay revealing the $AuNP_{40}$ induced apoptosis in lung cancer cells in a concentration dependent manner.

Table 4 Results of flow cytometric cell cycle and Annexin V assays with A549 cells incubated with $AuNP_{40}$ at different concentrations for 72 h. Live cell population alone was considered for cell cycle calculations

			Apoptotic cells %		
Concentration of $AuNP_{40}$	Sub G_0/G_1 %	G_0/G_1 %	Early	Late	Total
Control (0 pM)	4.3 ± 0.3	59.9 ± 1.4	2.39 ± 0.23	0.7 ± 0.14	3 ± 0.5
12.5 pM	26.0 ± 1.3	65.6 ± 1.8	16.07 ± 0.26	5.72 ± 0.57	22 ± 1
25.0 pM	41.2 ± 2.5	71.9 ± 1.1	17.68 ± 0.91	30.85 ± 0.74	47 ± 1

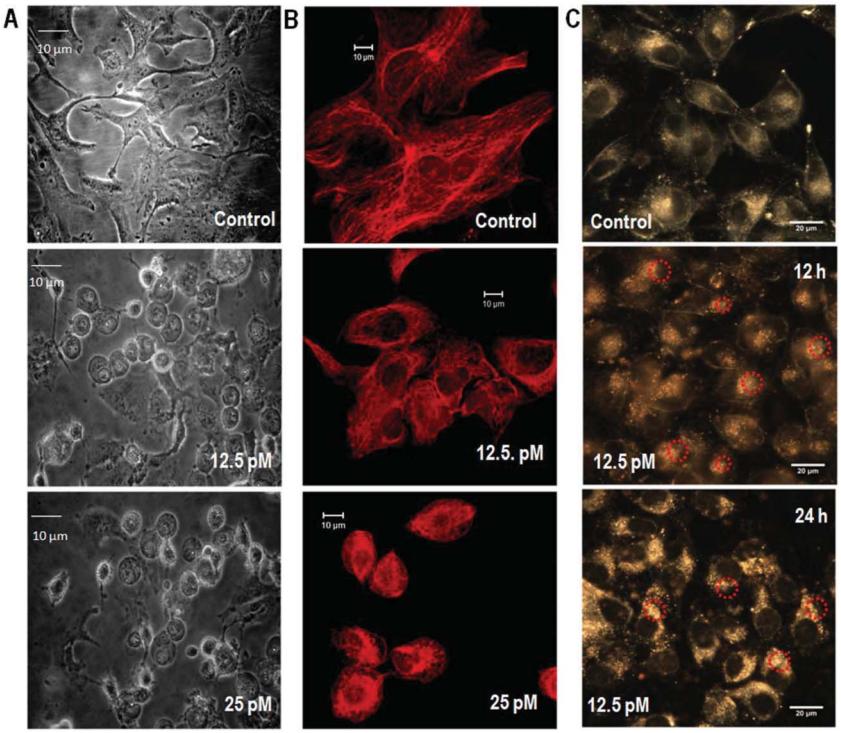

Fig. 6 (A) Phase contrast and (B) confocal images of control and $AuNP_{40}$ treated samples. $AuNP_{40}$ treated samples show MT damage while the control cells show a normal MT network after 72 h. (C) DFM images of the control and treated cells. The right top image is the control and the middle one is 25 pM $AuNP_{40}$ treated cells (incubation time 12 h) which show shrinkage when compared to the control. The right bottom is 12.5 pM $AuNP_{40}$-treated cells (for 24 h) showing more shrinkage than 12 h treated cells. In both 12 h treated and 24 h treated samples, scattering is seen which is distinctly different from that of scattering produced by vesicles in the normal, untreated cells (Fig. S9†). Some of the nanoparticles are labelled with dotted circles in the middle and bottom-most images of C.

morphology by phase contrast microscopy upon $AuNP_{40}$ treatment showed disruption of cell morphology and shrinkage of cellular periphery in a dose dependent manner (Fig. 6A). In phase contrast images, the observed MT network pattern in control samples was well distributed and extended, exhibiting a normal cytoskeletal structure while the $AuNP_{40}$ treated cells showed a damaged and shrunken MT network (Fig. 6B). 12.5 pM and 25.0 pM $AuNP_{40}$ treated cells were immunofluorescent stained with monoclonal anti-α-tubulin antibody and TRITC conjugated anti-mouse IgG secondary antibody. CLSM images were obtained to analyse the morphology. In 12.5 pM treated cells, peripheral MT were damaged and shrunken moderately while in 25.0 pM treated cells, the MT network was damaged extensively (Fig. 6B).

Recently, dark field microscopy (DFM) has been employed to probe the nanoparticle–cell interaction and to study the metabolic processes of cells, particularly in the presence of plasmonic nanoparticle-based smart-constructions to decipher the secrets of cells in real time.[62–64] The uptake of AuNPs by the cells was confirmed by DFM investigation using a hyperspectral imaging system. Hyperspectral imaging of the cells with NPs revealed that the particles were observed in the cytosol of the cell and not in the nucleus, though they were seen around the perinuclear membrane area (Fig. 6C and D). However, during the later period of incubation, nuclear morphology changes were observed, though no nanoparticles entered the nucleus. This can be attributed to the microtubule damage effect, as it is observed that microtubule-damaging drugs induce changes of nuclear morphology. Untreated cells also exhibited some scattering due to vesicles, but the cells with nanoparticles had higher plasmonic scattering which was distinctly different from that of scattering caused by vesicles (Fig. S9†). Shrinkage of the cytosolic portion of the cell was also observed with time (Fig. 6C, 12 h and 24 h). The positive control for MT damage was carried out with vinblastine, as it is known to destabilize MT and it was used for comparison (Fig. S10†).

To check whether actin also was damaged as a function of time, we stained both actin and tubulin with their respective antibodies and analysed in CLSM. In Fig. 7A it can be seen that after 12 and 24 h of incubation, MT (red) is more damaged and disrupted than actin (green) which leads to cell morphology change. To check whether $AuNP_{40}$ could cause aggregation of the tubulin–MT system intracellularly as well and whether the observed apoptosis is due to microtubule damage mediation, we carried out western blot. The experiment was carried out after giving cold shock to the formed microtubules (to the cell extract) which is necessary for depolymerization. A normal microtubule would depolymerize and give rise to tubulin monomers, but the aggregated tubulin–MT system would not become monomers. We compared the control cellular extract of treated and untreated cells by western blot after running in a 6% non-reducing SDS PAGE. We did not observe any aggregation of tubulin in the cellular extract collected from untreated cells (Fig. 7B, lane 1), while western blot of $AuNP_{40}$ treated cells

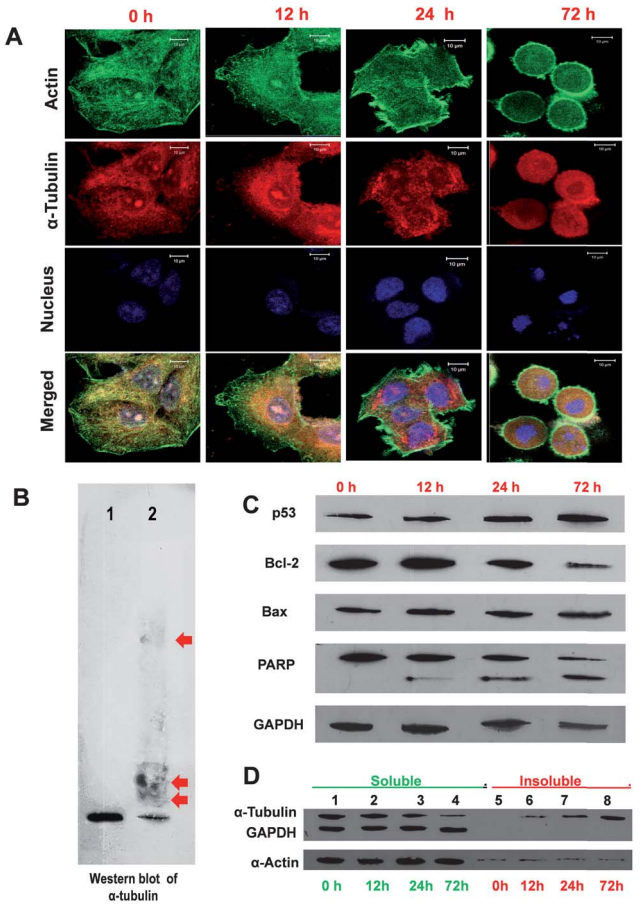

Fig. 7 (A) Confocal fluorescence images of A549 cells treated with $AuNP_{40}$ showing intracellular damage of microtubules as a function of time. Actin and tubulin microtubule are stained with their respective antibodies (actin-green and tubulin-red) and the nucleus is stained with DAPI. I, II, III and IV columns represent incubation times (with $AuNP_{40}$) of 0 h, 12 h, 24 h and 72 h, respectively. The scale bar is 10 μm. The positive control with vinblastine is provided in the ESI, Fig. S10.† (B) Western blot data showing non-aggregated tubulin in control cells (lane 1) and aggregated tubulin in AuNP treated cells (lane 2). (C) Western blot shows upregulation of apoptotic proteins p53 Bax/Bcl-2 and PARP cleavage (GADPH is the loading control). (D) Western blot done after cold depolymerization showing an increase in the aggregated insoluble tubulin while actin does not increase. The loading control GADPH does not aggregate suggesting that the microtubule was damaged and aggregated which induced concomitant cell cycle arrest and apoptosis.

showed tubulin aggregation (Fig. 7B, lane 2). In all cases protein aggregation sizes varied, suggesting that big tubulin aggregates are less likely to be stable and they easily disassociate when treated with SDS (Fig. 7B, lane 2). This signifies less involvement of covalent linkages (S–S, S–Au bonds), which is supported by the observation that less cysteine residues are modified due to AuNPs interaction (Fig. S7†). Hence, the aggregates may not be very stable in nature and easily get disrupted when treated by SDS. This indicates that the protein aggregates are not only formed due to covalent interactions with AuNPs but also due to weak interactions which have to be investigated in future to find the exact mechanism. Supporting the above view of weak interactions, in a study Zhou *et al.* have fabricated AuNPs in taxol polymerized MT, unlike the present study where direct AuNPs–tubulin interaction is monitored. They have reported that aromatic, imidazole group amino acids of tubulin and carboxylates can interact with AuNPs other than the thiol group of amino acids.[46] Results from *in vitro* intracellular experiments suggest that AuNPs interaction with the tubulin–MT system caused cell cycle arrest and apoptosis. Upregulation of proapoptotic proteins like p53 and Bax and down regulation of anti-apoptotic protein Bcl-2 were found (Fig. 7C). Cleavage of poly(ADP-ribose) polymerase (PARP), which is an indicator that the cell is undergoing apoptosis, was also observed (Fig. 7C). PARP is cleaved by caspases which are produced during mitochondrial apoptosis activation indicating that this is a mitochondrial apoptosis. It is known that microtubule damage induces caspase activation which leads to PARP cleavage as in the case of anti-MT drugs.[65] In Fig. 7A, after 24 h no differentiation between MT and actin damage can be made. Hence to check whether actin or other cellular protein also got aggregated (here we used the loading control), western blot was run after separating soluble and insoluble portions of the cell extract after cold depolymerization. WB results showed increase in tubulin aggregation in the insoluble part while actin and the loading control were not found in the insoluble part of the extract which also suggests that the microtubule is intracellularly damaged and aggregated (Fig. 7D). Another observation is that while the cells were highly viable for almost till 48 h (Fig. S11†) and only at 72 h the viability decreases largely and apoptosis is found; in confocal images at 24 h the initiation of damage of microtubules is clearly seen, which also reveals that the MT damage occurred before apoptosis and the observed apoptosis could be a MT-damage mediated one. It may also explain why we see an increasing ratio in PARP cleavage and other apoptotic signatures as a function of time along with increasing tubulin aggregates (Fig. 7C, D). Acetylation, a post translational modification, which can be one of the reasons for resistance to cold depolymerisation and increased half life of MT also could be ruled out. Upon acetylation, one would expect to see more stable, larger MT bundles (mostly near the cell membrane) without affecting the cell viability, but here instead we see disruption of MT leading to cell cycle arrest and apoptosis, further reinforcing the proposed hypothesis.[66,67] Culha and co-workers attempted to study AuNP-induced damage with the mitochondria of A549 cells; however they found no such damage, and reported that even incubating AuNPs with isolated mitochondria did not cause damage. They also suggested that AuNPs could have escaped the endosome and entered the cytosol in the A549 cell.[68] In a recent study, Dawson and co-workers found intracellular tubulin to be bound among many other bound proteins on the surface of silica and polymeric NPs incubated in the cytosolic fluid.[6] In the same study, they introduced the nanoparticles to human plasma (extracellular fluid) first and collected the particles. Then they subsequently introduced the particles to the cytosolic fluid and observed the binding of cytosolic proteins through re-equilibration of extracellular fluid proteins, revealing the dynamic nature and evolution of the protein corona while transferring from one biological fluid to another. This suggests that AuNPs could behave similarly, though they would interact with

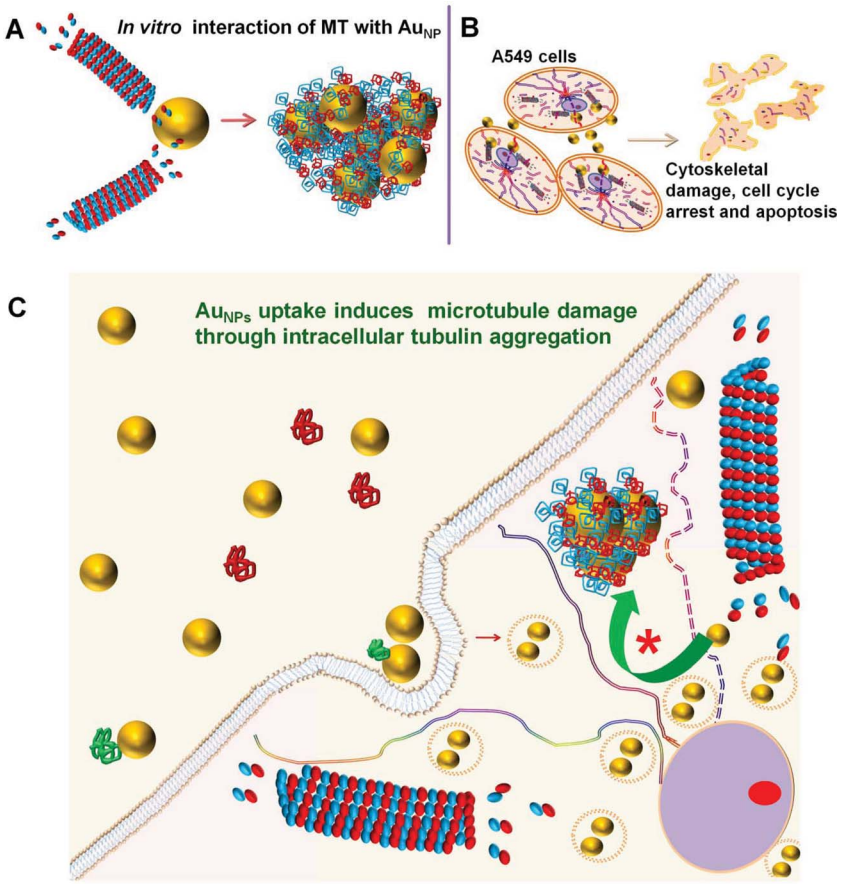

Scheme 1 (A) Representation of AuNPs-induced aggregation of the tubulin–MT system during the polymerization reaction. (B) AuNPs-induced apoptosis *in vitro* in the lung cancer cell line, A549. (C) Schematic of the uptake of AuNPs by A549 cells and insoluble aggregates of tubulin found inside the cell (* (red color) indicates that the intracellular aggregation mechanism is yet to be fully understood), while intracellular tubulin aggregation is clearly evident upon AuNP uptake (see Fig. 7D). The scheme is for illustration purpose only and not to scale.

proteins present in the media. Upon entry into the cell from the cell media or biological fluid, AuNPs could bind to intracellular proteins too through reassociation according to the relative affinities of the interacting proteins with the AuNP surface.[6] In neuronal progenitor cells, it has been observed that polymer coated AuNPs induced cytoskeletal damage.[69] Hence, in the light of the literature and from the observed results such as G_0/G_1 cell cycle arrest and aggregation of intracellular tubulin along with non-aggregation of intracellular actin or GADPH (a house keeping enzyme), it may be concluded that AuNPs interacted with tubulin inside the A549 cells and caused MT damage and subsequent cell cycle arrest and apoptosis. Although we have not studied how exactly AuNPs interact with MT inside the cell, MT damage and aggregation is evident from our observations (Fig. 7D). We also assume that the MT damage is likely to have initiated around the perinuclear region where crowding of AuNPs is seen (Fig. 6C) and where the MTs are nucleated and are densely organized. There are several reports indicating different routes of uptake (including non-specific and unknown routes) of AuNPs,[68,70] however, endocytosis facilitates the nanoparticle uptake prominently.[15] Endosomal escape of nanoparticles is an active area of research which is very important for delivery of drugs and genes. Here the observed effect could take place only if AuNPs escaped from the endosomes or through other unknown routes in which AuNPs were uptaken and have the probability to be present in the cytosol. Recently, Volk and co-workers have shown that gold nanoparticles could escape under low laser intensity (which is too low to cause a photothermal effect) without any photothermal effect from the endosomes and suggested that radical generation could facilitate such an escape.[71] During the late phases, upon maturation of endosomes, we assume that nanoparticles could likely escape.[72] Braeckamns and co-workers suggested that during the late phases the cytoskeleton may be damaged due to the crowding effect of growing nanoparticle containing endosomes.[69] The growth of endosomes upon crowding, ageing, non-thermal membrane disruption and steric effect could have likely resulted in the escape of particles.[61,71,72] However, detailed studies are required to answer these questions which are a subject of future investigation. Apoptosis itself could be caused by several pathways; however, here our observation of the presence of insoluble intracellular aggregation even after cold depolymerisation and the increasing quantity of insoluble aggregates as a function of time suggests a strong contribution of MT damage effect directed by AuNPs and it could be the predominant pathway in this case or one of the

several apotoptic pathways, since multiple toxic effects are seen when gold nanoparticles are uptaken.[69] Nevertheless, the involvement of MT damage in the toxicity effect is clear in the case of A549 cells. The key observations of the present study are illustrated in Scheme 1.

Further, how the presence of AuNPs affects the extracellular matrix and cellular adhesion during the incubation time, their concomitant signalling cascades and how they would in turn remodel or affect the MT would also give much clearer picture of what is happening inside the cell and it is an area of future investigation. We have observed similar effects in the case of the MCF-7 cell line also upon interaction with citrate capped AuNPs (Fig. S12 and S13† for cell viability and microtubule disruption, respectively), although these studies have been limited.

4 Summary and conclusions

In this paper, we have probed the nature of microtubule gold nanoparticle interaction, which has remained unaddressed till date and looked at the toxicity mechanism from the point of view of microtubule damage. Interaction of weakly protected AuNPs with tubulin in the cell free system was investigated in the first part of the study and we found that AuNPs can induce conformational-change-based aggregation in the tubulin–MT system, thus affecting the dynamic equilibrium. Extended aggregates of tubulin with AuNPs were seen by DFM and TEM. Second derivative IR and Raman spectroscopy revealed that partial conformational changes are responsible for the aggregation. Thus we have demonstrated, to the best of our knowledge till date, for the first time that conformational changes induced by the AuNP surface could lead to tubulin–MT aggregation. As the second part of the study, we have checked whether bare AuNPs could do the same inside the A549 cell. The observed experimental results such as G_0/G_1 cell cycle arrest and western blot showing intracellular aggregation of tubulin (while actin and GADPH do not show aggregation) hint that bare gold nanoparticles could cause MT damage-mediated cell cycle arrest and apoptosis in the lung cancer cell line A549, thus providing a plausible explanation for the elusive selective toxicity mechanism of AuNPs in the lung cancer cell line. NMR and computational studies to find the specific sites of tubulin interaction with AuNPs would be carried out in future. Similar studies may be done with engineered tubulin with green fluorescent protein (GFP) to know the *in situ* interaction in live cells. Although there are several reports indicating different uptake pathways of AuNPs, endocytosis plays a prominent role. The endosomal escape of AuNPs is important to cause the observed effects, hence cell biological and synthetic vesicles based studies investigating the bio-physicochemical parameters in which AuNPs' escape is facilitated would be a future study coupled with tubulin polymerization and non-endocytotic delivery experiments, which would help establish the intracellular tubulin aggregation mechanism. Removal of exocytosed AuNPs and quantification of endocytosed particles would also play a significant role in explaining the observed effect in future along with cell-cycle and cell-recovery based studies. We believe that this study offers a new insight into AuNP toxicity and would be useful in cancer therapeutics (where independent activity of AuNPs or the potential of AuNPs in synergy with MT cancer drugs could be harnessed to treat drug resistant lung and other cancer cells susceptible to AuNPs, since intracellular MT damaging property of AuNPs may not be resisted by drug resistant cancer cells) and understanding the safety of nanomaterials.

Acknowledgements

The work was supported by grants from DST, Govt of India (no. SR/SO/BB-14/2008) and the Nanoscience and Nanotechnology Program, University of Calcutta (sanction no. conv/042/NanoPr/2009) awarded to GC. Confocal microscope and FACS facilities were developed by the grant from the National Common Minimum Program, Govt of India. DC is supported by a fellowship from CSIR, Govt of India. DC thanks Dr Hirak Kumar Patra, Dept of Biochemistry, University of Calcutta for discussions. TP thanks the Department of Science and Technology, Government of India for constantly supporting his research program on nanomaterials.

References

1 A. E. Nel, L. Madler, D. Velegol, T. Xia, E. M. V. Hoek, P. Somasundaran, F. Klaessig, V. Castranova and M. Thompson, *Nat. Mater.*, 2009, **8**, 543–557.
2 G. Zuo, Q. Huang, G. Wei, R. Zhou and H. Fang, *ACS Nano*, 2010, **12**, 7508–7514.
3 Z. J. Deng, M. Liang, M. Monteiro, I. Toth and R. F. Minchin, *Nat. Nanotechnol.*, 2011, **6**, 39–44.
4 L. Calzolai, F. Franchini, D. Gilliland and F. Rossi, *Nano Lett.*, 2010, **10**, 3101–3105.
5 T. Cedervall, I. Lynch, S. Lindman, T. Berggård, E. Thulin, H. Nilsson, K. A. Dawson and S. Linse, *Proc. Natl. Acad. Sci. U. S. A.*, 2007, **104**, 2050–2055.
6 M. Lundqvist, J. Stigler, T. Cedervall, T. Berggard, M. B. Flanagan, I. Lynch, G. Eliaz and K. Dawson, *ACS Nano*, 2011, **5**, 7503–7509.
7 V. L. Colvin and K. M. Kulinowski, *Proc. Natl. Acad. Sci. U. S. A.*, 2007, **104**, 8679–8680.
8 L. Fei and S. Perrett, *Int. J. Mol. Sci.*, 2009, **10**, 646–655.
9 D. Zhang, O. Neumann, H. Wang, V. M. Yuwono, A. Barhoumi, M. Perham, J. D. Hartgerink, P. Wittung-Stafshede and N. J. Halas, *Nano Lett.*, 2009, **2**, 666–671.
10 P. L. Xavier, K. Chaudhari, P. K. Verma, S. K. Pal and T. Pradeep, *Nanoscale*, 2010, **2**, 2769–2776.
11 W. Shang, J. H. Nuffer, V. A. Muñiz-Papandrea, W. Colón, R. W. Siegel and J. S. Dordick, *Small*, 2009, **5**, 470–476.
12 S. J. Soenen, P. Rivera-Gil, J. M. Montenegro, W. J. Parak, S. C. D. Smedt and K. Braeckmans, *Nano Today*, 2011, **6**, 446–465.
13 H. D. Summers, P. Rees, M. D. Holton, M. R. Brown, S. C. Chappell, P. J. Smith and R. J. Errington, *Nat. Nanotechnol.*, 2011, **6**, 170–174.
14 T. G. Iversen, T. Skotland and K. Sandvig, *Nano Today*, 2011, **6**, 176–185.

15 R. Lévy, U. Shaheen, Y. Cesbron and V. Sée, *Nano Rev.*, 2010, **1**, 4889.
16 E. C. Dreaden, A. M. Alkilany, X. Huang, C. J. Murphy and M. A. El-Sayed, *Chem. Soc. Rev.*, 2012, **41**, 2740–2779.
17 P. Ghosh, G. Han, M. De, C. K. Kim and V. M. Rotello, *Adv. Drug Delivery Rev.*, 2008, **60**, 1307–1315.
18 B. Kang, M. A. Mackey and M. A. El-Sayed, *J. Am. Chem. Soc.*, 2010, **132**, 1517–1519.
19 S. Mallidi, T. Larson, J. Tam, P. P. Joshi, A. Karpiouk, K. Sokolov and S. Emelianov, *Nano Lett.*, 2009, **9**, 2825–2831.
20 S. Dhar, V. Mali, S. Bodhankar, A. Shiras, B. L. V. Prasad and V. Pokharkar, *J. Appl. Toxicol.*, 2011, **5**, 411–420.
21 J. Nam, N. Won, H. Jin, H. Chung and S. Kim, *J. Am. Chem. Soc.*, 2009, **131**, 13639–13645.
22 W. Lu, S. R. Arumugam, D. Senapati, A. K. Singh, T. Arbneshi, S. A. Khan, H. Yu and P. C. Ray, *ACS Nano*, 2010, **4**, 1739–1749.
23 X. Huang, P. K. Jain, I. H. El-Sayed and M. A. El-Sayed, *Lasers Med. Sci.*, 2008, **23**, 217–228.
24 C. A. Simpson, B. J. Huffman, A. E. Gerdon and D. E. Cliffel, *Chem. Res. Toxicol.*, 2010, **23**, 1608–1616.
25 Y. Zhao, X. Gu, H. Ma, X. He, M. Liu and Y. Ding, *J. Phys. Chem. C*, 2011, **115**, 12797–12802.
26 N. M. Schaeublin, L. K. Braydich-Stolle, A. M. Schrand, J. M. Miller, J. Hutchison, J. J. Schlager and S. M. Hussain, *Nanoscale*, 2011, **3**, 410–420.
27 H. K. Patra, S. Banerjee, U. Chaudhuri, P. Lahiri and A. K. Dasgupta, *Nanomedicine*, 2007, **3**, 111–119.
28 C. Grabinski, N. Schaeublin, A. Wijaya, H. D'Couto, S. H. Baxamusa, K. H. Schifferli and S. M. Hussain, *ACS Nano*, 2011, **5**, 2870–2879.
29 T. S. Hauck, A. A. Ghazani and W. C. Chan, *Small*, 2008, **4**, 153–159.
30 S. Wang, W. Lu, O. Tovmachenko, U. S. Rai, H. Yu and P. C. Ray, *Chem. Phys. Lett.*, 2008, **463**, 145–149.
31 J. A. Khan, B. Pillai, T. K. Das, Y. Singh and S. Maiti, *ChemBioChem*, 2007, **8**, 1237–1240.
32 K. H. Downing and E. Nogales, *Curr. Opin. Cell Biol.*, 1998, **10**, 16–22.
33 M. A. Jordan and L. Wilson, *Nat. Rev. Cancer*, 2004, **4**, 253–265.
34 K. H. Downing, *Annu. Rev. Cell Dev. Biol.*, 2000, **16**, 89–111.
35 N. Kumar, *J. Biol. Chem.*, 1981, **256**, 10435–10441.
36 S. S. Rai and J. Wolff, *J. Biol. Chem.*, 1996, **271**, 14707–14711.
37 B. R. Acharya, D. Choudhury, A. Das and G. Chakrabarti, *Biochemistry*, 2009, **48**, 6963–6974.
38 P. B. Mullan, J. E. Quinn, P. M. Gilmore, S. McWilliams, H. Andrews, C. Gervin, N. McCabe, S. McKenna, P. White, Y. H. Song, S. Maheswaran, E. Liu, D. A. Haber, P. G. Johnston and D. P. Harkin, *Oncogene*, 2001, **20**, 6123–6131.
39 M. Hari, F. Loganzo, T. Annable, X. Tan, S. Musto, D. B. Morilla, J. H. Nettles, J. P. Snyder and L. M. Greenberger, *Mol. Cancer Ther.*, 2006, **5**, 270–278.
40 D. Choudhury, A. Das, A. Bhattacharya and G. Chakrabarti, *Food Chem. Toxicol.*, 2010, **48**, 2872–2880.
41 A. A. Sablina, L. S. Agapova, M. P. Chumakov and B. P. Kopnin, *Cell Biol. Int.*, 1999, **23**, 323–334.
42 S. H. Khan and G. M. Wahl, *Cancer Res.*, 1998, **58**, 396–401.
43 Z. N. Gheshlaghi, G. H. Riazi, S. Ahmadian, M. Ghafari and R. Mahinpour, *Acta Biochim. Biophys. Sin.*, 2008, **40**, 777–782.
44 J. C. Zhou, X. Wang, M. Xue, Z. Xu, T. Hamasaki, Y. Yang, K. Wang and B. Dunn, *Mater. Sci. Eng., C*, 2010, **30**, 20–26.
45 P. L. Apopa, Y. Qian, R. Shao, N. L. Guo, D. Schwegler-Berry, M. Pacurari, D. Porter, X. Shi, V. Vallyathan, V. Castranova, *et al.*, *Part. Fibre Toxicol.*, 2009, **6**, 1–14.
46 T. A. Ratnikova, P. N. Govindan, E. Salonen and P. C. Ke, *ACS Nano*, 2011, **5**, 6306–6314.
47 J. Kimling, M. Maier, M. B. Okenve, V. Kotaidis, H. Ballot and A. Plech, *J. Phys. Chem. B*, 2006, **110**, 15700–15707.
48 M. M. Bradford, *Anal. Biochem.*, 1976, **72**, 248–254.
49 M. Roychowdhury, N. Sarkar, T. Manna, S. Bhattacharyya, T. Sarkar, P. Basusarkar, S. Roy and B. Bhattacharyya, *Eur. J. Biochem.*, 2000, **267**, 3469–3476.
50 D. Hall and A. P. Minton, *Anal. Biochem.*, 2005, **345**, 198–213.
51 S. Mukherjee, B. R. Acharya, B. Bhattacharyya and G. Chakrabarti, *Biochemistry*, 2010, **49**, 1702–1712.
52 T. Deb, D. Choudhury, P. S. Guin, M. B. Saha, G. Chakrabarti and S. A. Das, *Chem.–Biol. Interact.*, 2011, **189**, 206–214.
53 J. R. Lakowicz, *Principles of Fluorescence Spectroscopy*, Kluwer Academic/Plenum Publishers, New York, 2nd edn, 1999.
54 S. K. Ghosh and T. Pal, *Chem. Rev.*, 2007, **107**, 4797–4862.
55 C. F. B. Séné, M. C. McCann, R. H. Wilson and R. Crinter, *Plant Physiol.*, 1994, **106**, 1623–1631.
56 T. G. Spiro and F. J. Farrell, *Inorg. Chem.*, 1971, **10**, 1606–1610.
57 S. H. Brewer, W. R. Glomm, M. C. Johnson, M. K. Knag and S. Franzen, *Langmuir*, 2005, **21**, 9303–9307.
58 A. Albanese, P. S. Tang and W. C. W. Chan, *Annu. Rev. Biomed. Eng.*, 2012, **12**, 1–16.
59 B. D. Chithrani, A. A. Ghazani and W. C. W. Chan, *Nano Lett.*, 2006, **6**, 662–668.
60 S. H. Wang, C. W. Lee, A. Chiou and P. K. Wei, *J. Nanobiotechnol.*, 2010, **8**, 33.
61 M. R. R. D. Planque, S. Aghdaei, T. Roose and H. Morgan, *ACS Nano*, 2011, **5**, 3599–3606.
62 Y. Jun, S. Sheikholeslamia, D. R. Hostetter, C. Tajon, C. S. Craik and A. P. Alivisatos, *Proc. Natl. Acad. Sci. U. S. A.*, 2009, **106**, 17735–17740.
63 N. Liu, M. Hentschel, T. Weiss, A. P. Alivisatos and H. Giessen, *Science*, 2011, **332**, 1407–1410.
64 L. Zhang, Y. Li, D. W. Li, C. Jing, X. Chen, M. Lv, Q. Huang, Y. T. Long and I. Willner, *Angew. Chem., Int. Ed.*, 2011, **50**, 6789–679.
65 R. K. Srivastava, A. R. Srivastava, S. J. Korsmeyer, M. Nesterova, Y. S. Cho-Chung and D. L. Longo, *Mol. Cell. Biol.*, 1998, **18**, 3509–3517.
66 Y. Zilberman, C. Ballestrem, L. Carramusa, R. Mazitschek, S. Khochbin and A. Bershadsky, *J. Cell Sci.*, 2009, **122**, 3531–3541.

67 S. Kapoor and D. Panda, *Biochem. Pharmacol.*, 2012, **83**, 1495–506.
68 Ö. F. Karataş, E. Sezgin, Ö. Aydın and M. Çulha, *Colloids Surf., B*, 2009, **71**, 315–318.
69 S. J. Soenen, B. Manshian, J. M. Montenegro, F. Amin, B. Meermann, T. Thiron, M. Cornelissen, F. Vanhaecke, S. Doak, W. J. Parak, S. D. Smedt and K. Braeckmans, *ACS Nano*, 2012, **6**, 5767–5783.
70 A. França, P. Aggarwal, E. V. Barsov, S. V. Kozlov, M. A. Dobrovolskai and Á. G. Fernández, *Nanomedicine*, 2011, **6**, 1175–88.
71 Z. Krpetic, P. Nativo, V. See, I. A. Prior, M. Brust and M. Volk, *Nano Lett.*, 2010, **10**, 4549–4554.
72 T. Mironava, M. Hadjiargyrou, M. Simon, V. Jurukovski and M. H. Rafailovichi, *Nanotoxicology*, 2010, **4**, 120–137.

